

# Synthesis of CuS nanoparticles by a wet chemical route and their photocatalytic activity

Mou Pal · N. R. Mathews · E. Sanchez-Mora ·  
U. Pal · F. Paraguay-Delgado · X. Mathew

Received: 21 February 2015 / Accepted: 3 July 2015 / Published online: 11 July 2015  
© Springer Science+Business Media Dordrecht 2015

**Abstract** CuS nanoparticles (NPs) of few nanometers in size were prepared by a wet chemical method. The structural, compositional, and optical properties of the NPs were characterized by X-ray diffraction (XRD), scanning electron microscopy, transmission electron microscopy, energy-dispersive X-ray spectroscopy, micro Raman and Fourier transform infrared spectroscopy, N<sub>2</sub> adsorption–desorption isotherms, and UV–Vis diffuse reflectance spectroscopy. The XRD pattern proved the presence of hexagonal phase of CuS particles which was further supported by Raman spectrum. The estimated band gap energy of 2.05 eV for the slightly sulfur-rich CuS NPs is relatively larger than that of bulk CuS (1.85 eV), indicating the small size effect. As-prepared NPs showed excellent photocatalytic activity for the degradation of methylene blue (MB) under visible light. The surface-bound OH<sup>-</sup> ions at the CuS

nanostructures help adsorb MB molecules facilitating their degradation process under visible light illumination. The studies presented in this paper suggest that the synthesized CuS NPs are promising, efficient, stable, and visible-light-sensitive photocatalyst for the remediation of wastewater polluted by chemically stable azo dyes such as MB.

**Keywords** CuS · Photocatalysis · Nanoparticles · Modeling and simulations · Environmental and health effects

## Introduction

Over the past few decades, semiconductor nanoparticles are receiving considerable attention in the area of environmental remediation technology due to their great potential as heterogeneous photocatalysts (Hoffmann et al. 1995; Zhang et al. 2011; Meng et al. 2013). The increased water pollution from different sources such as industrial effluents, chemical spills, and agricultural runoff poses a serious threat to human health and environment. In this context, TiO<sub>2</sub> has been applied extensively in the treatment of organic pollutants due to its non-toxicity, low material cost, photochemical stability, and outstanding performance in photodegradation (Linsebigler et al. 1995; Nagaveni et al. 2004; Daghrir et al. 2013). However, due to its wide band gap, pure TiO<sub>2</sub> is sensitive only to UV light and unable to make effective utilization of major

---

M. Pal · N. R. Mathews · X. Mathew (✉)  
Instituto de Energías Renovables, Universidad Nacional  
Autónoma de México, 62580 Temixco, Morelos, Mexico  
e-mail: xm@ier.unam.mx

M. Pal · E. Sanchez-Mora · U. Pal  
Instituto de Física, BUAP, Av. San Claudio y Blvd. 18 Sur  
Col. San Manuel, Ciudad Universitaria,  
C.P. 72570 Puebla, Mexico

F. Paraguay-Delgado  
Departamento de Materiales Nanoestructurados, Centro  
de Investigación en Materiales Avanzados (CIMAV),  
Chihuahua, Mexico

part of the sunlight. To exploit maximum solar energy, it is important to employ semiconductors with absorption in the visible light range as photocatalysts. Transition metal chalcogenides are found to be promising for this purpose as they have inherent ability to absorb light in the visible and near infrared regions (Gorai et al. 2005; Xiong et al. 2010; Guo et al. 2011). Copper sulfides with various stoichiometries are important p-type semiconductors of this series with technological applications in solar cells (Mane and Lokhande 2000), optical filters (Li et al. 2002), lithium rechargeable batteries (Han et al. 2011), catalysis (Meng et al. 2013; Basu et al. 2010), and gas sensing (Setkus et al. 2001). Specifically, covellite CuS, a greenish black solid, is of particular interest to the researchers as it shows metal-like conductivity and chemical sensing capacity and can be transformed into superconductor at a low temperature of 1.6 K (Zhang et al. 2003; Ou et al. 2005). It has a hexagonal crystalline structure, made of layers of planar  $\text{CuS}_3$  triangles with  $\text{Cu}^{2+}$  and  $\text{S}^{2-}$  ions surrounded by  $\text{CuS}_4$  tetrahedron of  $\text{Cu}^+$  and  $\text{S}_2^{2-}$  ions (Kumar et al. 2013). Recently, CuS nanoparticles have been used as photocatalysts for the degradation of organic dyes such as MB, methyl red, methyl orange, Rhodamine B, and 2,4-dichlorophenol. While Meng et al. found effective catalytic property for the degradation of Rhodamine B and 2,4-dichlorophenol using hierarchical CuS hollow nanospheres (Meng et al. 2013), Basu et al. have studied the photocatalytic degradation of different dye molecules under visible light with hexagonal stacked plates of CuS (Basu et al. 2010). Gupta et al. explored the novelty of pectin–CuS nanocomposite structure for dye degradation utilizing the ability of pectin as a bio-adsorbent and CuS as a photocatalyst (Gupta et al. 2012). Shu et al. developed porous hollow CuS nanomaterials as artificial enzymes showing excellent peroxidase-like catalytic activity (Shu et al. 2015). To date, different techniques have been developed to prepare CuS nanocrystals including template-mediated growth (Wu et al. 2013), hydrothermal (Wang et al. 2009), solvothermal (Meng et al. 2013, Kumar et al. 2011), thermolysis (Chen et al. 2008), wet chemical method (Roy and Srivastava 2007), polyol route (Shen et al. 2003), solid-state reaction (Wang et al. 2006), and sonochemical methods (Deng et al. 2014). Many of the aforementioned synthetic methods face disadvantages such as need of high temperature, harsh reaction conditions, use of

template material which may leave impurities, low reaction yield restricting their large-scale production, and the presence of undesired secondary phases. Therefore, synthesis of phase-pure CuS nanostructures with desired Cu:S ratio by a solution-based low-cost method is still a challenging task.

Herein, we report the synthesis of sub-10-nm-size covellite CuS nanocrystals in large quantities by a cost-effective wet chemical route. The structural, optical, and photocatalytic properties of the product were thoroughly characterized. As-synthesized CuS nanoparticles have demonstrated rapid dye adsorption as well as excellent photodegradation capacity in aqueous solution.

## Experimental

### Material synthesis

CuS nanoparticles were synthesized by a wet chemical route using triethanolamine (TEA) as a complexing agent. The precursor solution was prepared by sequential addition of 15 mL of 0.5 M  $\text{CuCl}_2$  (Sigma, 99 %), 5 mL of TEA (J. T. Baker, 99.87 %), 10 mL of  $\text{NH}_4\text{OH}$  (J. T. Baker, 28–30 %), 10 mL of 1 M NaOH (Sigma-Aldrich), 15 mL of 0.5 M thiourea solution (Sigma-Aldrich, 99 %), and deionized water to make the final volume of 100 mL. The mixture was magnetically stirred at 50 °C for 1 h in an oil bath. The resulting precipitate was separated by centrifugation, washed repeatedly with deionized water and ethanol, and dried overnight at room temperature to get the dark greenish powder sample. In each batch of synthesis, we obtained approximately 800 mg of CuS NPs.

### Characterization

Crystal structure of the as-synthesized sample was studied using its X-ray powder diffraction data obtained on a Rigaku X-ray diffractometer using monochromatized  $\text{CuK}\alpha$  radiation ( $K\alpha = 1.54056 \text{ \AA}$ ). The  $2\theta$  scanning rate was  $1.2 \text{ s step}^{-1}$  with a step size of  $0.02^\circ$ . The morphology and chemical composition of the product were examined with a field emission scanning electron microscope (FESEM, Hitachi S-5500) equipped with an energy-dispersive X-ray spectroscopy (EDS) accessory

(Bruker Quantax), operating at 5 kV. The TEM images were obtained with a JEOL (JEM 2200FS) microscope, operating at 300 kV accelerating voltage. Raman spectrum of the powder sample was recorded using a JobinYvon RAM HR800 Raman spectrometer equipped with an Olympus BX41 microscope and a charge-coupled device as a detector. The 632.8 nm emission of an He–Ne laser was used as the excitation source. UV–Vis diffuse reflectance (DR) spectrum of the powder sample was obtained in a Varian Cary 100 UV–Vis spectrophotometer equipped with DRA-CA-30I diffuse reflectance accessory, using MgO as reference. Nitrogen adsorption–desorption isotherm of the sample was collected on a Belsorp-Mini II (BEL Japan, Inc) analyzer. The sample was degassed at 100 °C for 5 h in vacuum prior to the measurement. Infrared spectrum of the sample was recorded using an Equinox-55 FT-IR spectrometer (Bruker) in the range of 400–4000  $\text{cm}^{-1}$  with a resolution of 4  $\text{cm}^{-1}$ . For this, approximately 15 mg of powder sample was placed into the groove of the sample holder without using KBr or other additives.

#### Evaluation of photocatalytic activity

Photocatalytic property of CuS powder was evaluated by degrading methylene blue (MB) ( $\text{C}_{16}\text{H}_{18}\text{ClN}_3\cdot\text{S}\cdot 3\text{H}_2\text{O}$ , Sigma-Aldrich) as a test contaminant in aqueous solution under visible light irradiation. The photocatalytic experiment was conducted in a home-made reactor by dispersing 30 mg of CuS powder sample into 100 mL of MB solution (15  $\text{mg L}^{-1}$ ). Oxygen was bubbled through the reaction mixture during the experiment. The dispersion was kept in dark under stirring for 1 h to establish adsorption/desorption equilibrium, and at given time intervals 5 mL of aliquot was withdrawn from the reactor in order to determine the adsorption of MB over the photocatalyst surface. Afterwards, the catalyst containing MB solution was irradiated by visible light using a 10 W LED lamp (model HH-10WB1GB33 M) with predominant emission at  $\lambda = 440$  nm. The distance between the lamp and the test solution surface was set to be 10 cm, and the reaction temperature was maintained at 25 °C using a water jacket. During illumination, 5 mL of aliquot was pipetted out from the suspension at an interval of 30 min and centrifuged to separate the catalyst. The decolorization of MB was monitored by analyzing the absorption of the

supernatant solution at the maximum absorption wavelength of MB (664 nm) using a Varian Cary 100 UV–Vis spectrophotometer. The concentration of MB in the solution was determined using a previously established calibration curve.

#### Qualitative determination of Lewis basicity

To determine the Lewis basicity of the catalyst, the pH variation as a function of time was studied by dispersing 100 mg of CuS sample into 25 ml of 0.005 M HCl solution. The pH was monitored at regular intervals for 1 h keeping the CuS dispersion under constant and mild agitation. The variation of solution pH was recorded until the equilibrium was established. The number of -OH groups (density) per gram of the CuS catalyst was calculated following the method described elsewhere (Corro et al. 2014).

#### Evaluation of the Cu leaching into the reaction solution during photocatalytic process

To study the stability of CuS nanoparticles during photocatalytic process, the concentration of Cu ions released into the MB solution was monitored using Inductively Coupled Plasma-Atomic Emission Spectrometer (ICP-AES, ULTIMA 2, Horiba Scientific). At the end of the whole catalytic reaction, including dark and light periods, 10 mL of the aliquot was pipetted out and subjected to centrifugation to remove the dispersed catalyst. The supernatant was analyzed by ICP method; side by side a blank test was also done with the deionized water which was used to prepare the aqueous solution of MB.

## Results and discussion

#### Structural and morphological characterization

##### *X-ray diffraction analysis*

The diffraction peaks (Fig. 1) match well with the reflections reported for the hexagonal CuS (JCPDS # 06-0464). The main diffraction peaks observed at  $2\theta$  values of 27.9°, 29.4°, 32.9°, and 48.0° correspond to the lattice planes (101), (102), (006), and (110), respectively, while the minor peaks could be indexed as (103), (108), (201), (202), (203), and (116) planes of

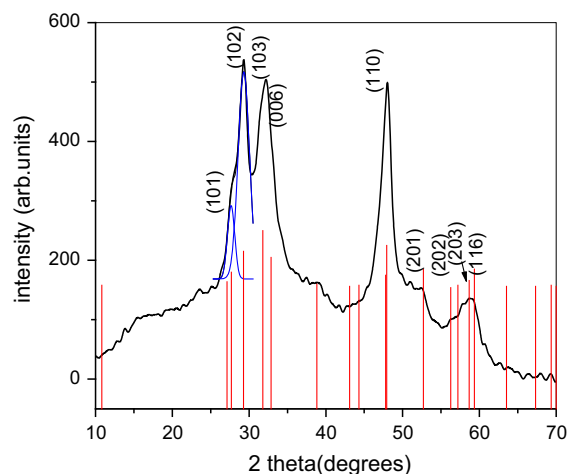


**Fig. 1** Powder X-ray diffraction patterns of CuS nanoparticles synthesized by the wet chemical method

covellite CuS. In general, the peaks are broad in nature indicating the formation of particles with small crystallite size. The estimated lattice parameters extracted from the diffraction data are  $a = b = 3.785 \text{ \AA}$  and  $c = 16.423 \text{ \AA}$  which are close to the reported values (Roy and Srivastava 2007). The average crystalline size was estimated using Debye–Scherrer equation:

$$D = \frac{k\lambda}{\beta \cos \theta},$$

where  $D$  is the crystallite size,  $\lambda$  is the wavelength of the incident radiation,  $k$  is the geometrical factor which is considered to be 0.90 in the case of spherical crystals,  $\theta$  is the Bragg angle taken in radians, and  $\beta$  is the full width at half maximum (FWHM) in radians. Utilizing the FWHM of the deconvoluted diffraction band associated to (102) crystalline plane, the average crystallite size in the sample was estimated to be 4.54 nm.

#### SEM and TEM study

The size and morphology of the as-grown CuS nanoparticles have been studied using FESEM and TEM. In Fig. 2, panels (a) and (c) show SEM and TEM images of CuS NPs, respectively; the formation of individual spherical particles as well as the aggregated species with nearly uniform diameter can be appreciated in both figures. The mean size and standard deviation (SD) of the nanoparticles were

estimated from the SEM image by measuring a population of approximately 80 particles as shown in Fig. 2b. The average diameter of the spherical CuS nanocrystals is close to  $4.7 \pm 0.25 \text{ nm}$ , suggesting a narrow size distribution ( $SD \approx 5 \%$ ).

The elemental composition of the powder sample was determined by EDS elemental analysis, and the spectrum is shown in the inset of Fig. 2a. The atomic percent of Cu and S are 47.63 and 52.37 %, respectively. The copper-deficient composition of the sample is the characteristic of covellite phase (Jiang et al. 2000).

To get a deep insight into the structure of the NPs, HRTEM analysis was performed. The image (Fig. 2d) shows the well-defined atomic planes with a lattice fringe spacing of  $2.82 \text{ \AA}$ , corresponding to (103) plane of hexagonal CuS phase. The inset of Fig. 2d highlights the FFT pattern, consisting of the bright spots which can be indexed as (103) diffraction plane of covellite CuS (JCPDS# 06-0464).

#### Raman spectroscopic study

Among many stable copper sulfide phases (CuS,  $\text{Cu}_{1.75}\text{S}$ ,  $\text{Cu}_{1.95}\text{S}$ ,  $\text{Cu}_2\text{S}$ ), Raman spectra of covellite phase (CuS) have mainly been reported. According to literature, the thermal sensitivity, metal-like conductivity, and fluorescence property make it difficult to obtain reliable Raman spectra from other copper sulfide phases. Figure 3 displays the Raman spectrum of CuS nanoparticles. The sharp band at  $468 \text{ cm}^{-1}$  is attributed to S–S stretching vibration, while a weak band at  $263 \text{ cm}^{-1}$  corresponds to  $A_{1g}$  TO mode. Both of these peaks have been associated with the covellite phase of CuS (Munce et al. 2007; Safrani et al. 2013).

We believe that the successful formation of uniform and pure covellite phase of CuS nanoparticles with an average diameter of approximately 5 nm is possible due to the utilization of triethanolamine as a complexing agent. Similar results have been reported by Xu et al. for the synthesis of monodisperse SnS quantum dots where TEA was used as a complexing ligand (Xu et al. 2009). Being a tetradentate ligand containing three –OH and a lone pair of electrons localized on the N atom, it forms a stable  $[\text{Cu}(\text{TEA})_n]^{2+}$  complex with metal ions ( $n$  is the coordination number of metal ion) (Panigrahi and Pathak 2013). The formation of this complex ion is highly favorable in order to control the reaction

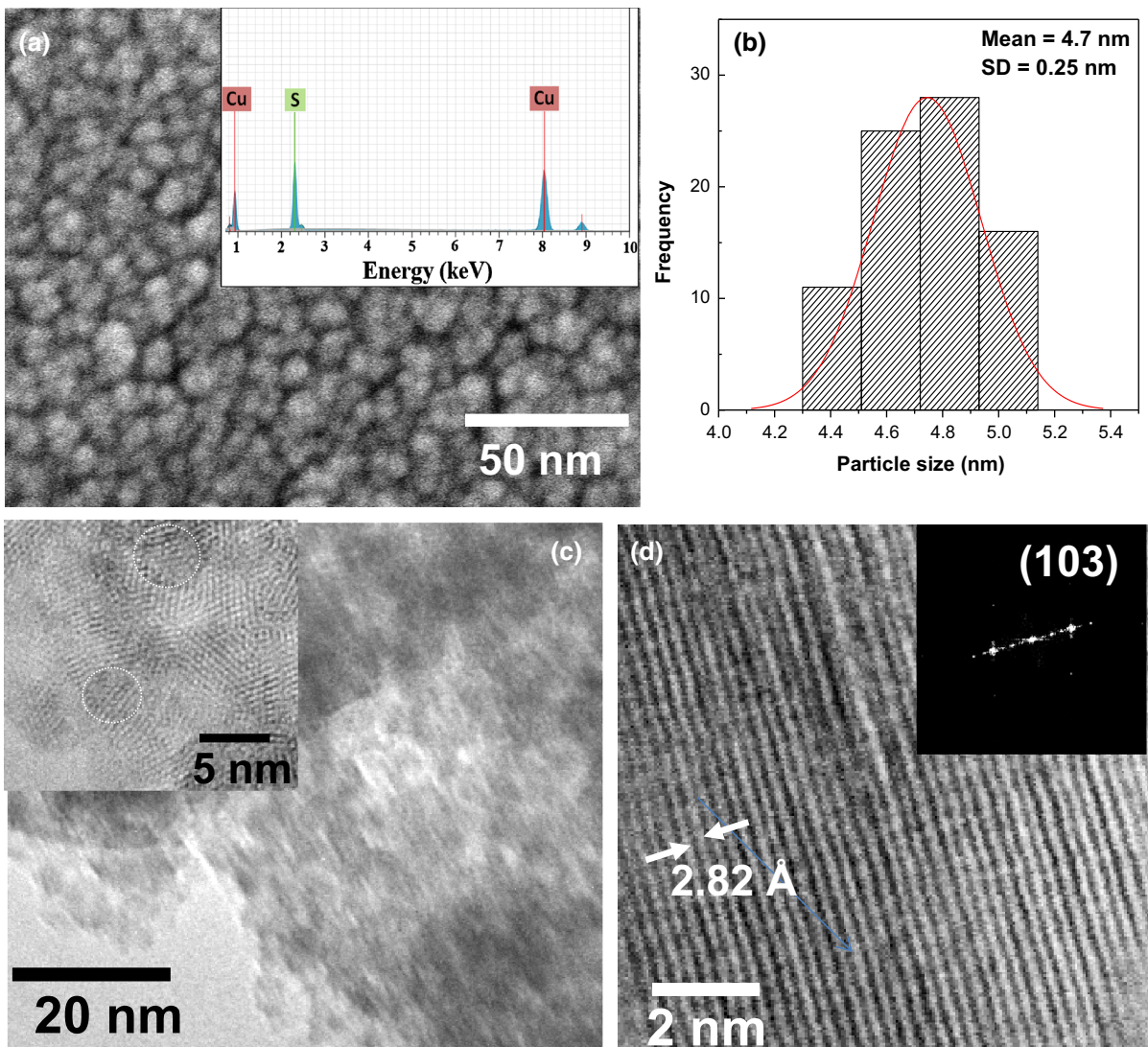
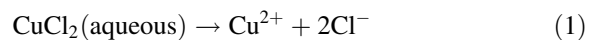


**Fig. 2** FESEM (a) and TEM (c) images showing spherical morphology of as-grown nanoparticles, *inset* of (c) is the high-resolution image of some CuS particles; (b) the size distribution histogram obtained from SEM image. EDS spectrum of CuS

kinetics as it avoids the immediate precipitation of  $\text{Cu}^{2+}$  ions in the solution when the precipitating anions such as  $\text{S}^{2-}$  are added to it. Also the metal-ion chelation process prevents the formation of  $\text{Cu}(\text{OH})_2$  under strong alkaline condition. Initially, TEA forms stable complexes with  $\text{Cu}^{2+}$  ions resulting from the dissociation of copper (II) chloride in water. On the other hand, thiourea, at high pH, undergoes slow hydrolysis to form  $\text{S}^{2-}$  ions. In turn, precipitation of CuS would occur when the product of ionic concentrations  $[\text{Cu}^{2+}][\text{S}^{2-}]$  exceeds the solubility product

NPs is shown in the *inset* of (a); (d) the HRTEM image showing well-resolved lattice planes. *inset* of d is the corresponding fast Fourier transform patterns confirming the covellite phase of CuS

( $K_{SP}$ ) of CuS (Liufu et al. 2008). The whole process can be described by the following set of chemical equations:



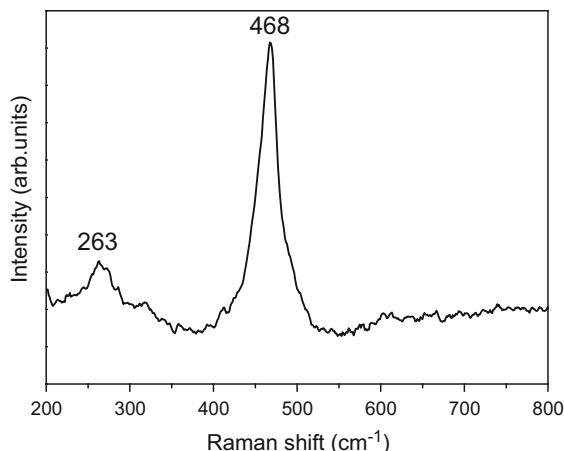


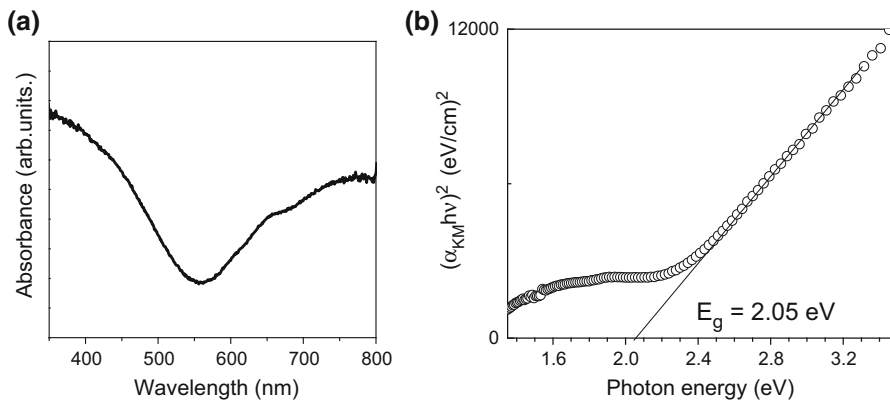
**Fig. 3** Raman spectrum of CuS nanocrystals

Although, there exists the possibility of forming copper hydroxides due to the excess concentration of  $\text{OH}^-$  ions, they would be spontaneously converted into CuS as the solubility product of CuS phase is much lower than that of  $\text{Cu}(\text{OH})_2$  ( $K_{\text{SP}(\text{CuS})} = 6 \times 10^{-37}$ ,  $K_{\text{SP}(\text{Cu}(\text{OH})_2)} = 2.2 \times 10^{-20}$ ).

#### Optical characterization

Figure 4 shows the UV–Vis absorption spectrum of CuS powder sample recorded in diffuse reflectance mode. From the absorption spectrum, we can clearly see that the sample absorbs strongly in the spectral region between 400 and 550 nm (Fig. 4a). The broad shoulder in the 650–750 nm range can be attributed to the d–d transition of Cu(II) state and is a general characteristic

**Fig. 4** **a** UV–Vis diffuse reflectance absorption spectrum of CuS nanoparticles, **b** plot of  $(\alpha_{\text{KM}}h\nu)^2$  versus  $h\nu$  for estimating the optical band gap of CuS powder sample



of covellite phase (Roy and Srivastava 2007; Qiu et al. 2010). The reflectance spectrum was analyzed by Kubelka–Munk formalism to obtain equivalent absorption coefficient ( $\alpha_{\text{KM}}$ ) using the relation:

$$\alpha_{\text{KM}} = (1 - R_\infty)^2 / 2R_\infty,$$

where  $R_\infty$  is the reflectance of an infinitely thick sample with respect to a reference at each wavelength. The optical band gap of CuS was calculated from  $\alpha_{\text{KM}}$  using the following equation associated with the direct transition:

$$\alpha_{\text{KM}}h\nu = A(h\nu - E_g)^{1/2},$$

where  $h\nu$  is the photon energy,  $A$  is a constant, and  $E_g$  is the band gap. A plot of  $(\alpha_{\text{KM}}h\nu)^2$  versus  $h\nu$  is shown in Fig. 4b; the extrapolated linear portion of the plot to photon energy axis gives the  $E_g$  value of CuS as 2.05 eV which is relatively larger than the reported band gap value of bulk CuS (1.85 eV), indicating small size effect (Basu et al. 2010).

#### $\text{N}_2$ adsorption–desorption study

Figure 5 shows the  $\text{N}_2$  adsorption–desorption isotherm of the CuS sample. As can be seen, the isotherm shows a hysteresis loop of type IV at relative pressure ( $P/P_0$ ) between 0.6 and 1.0 indicating the presence of mesopores. The mesopores were probably formed by the interconnection or aggregation of small nanoparticles which is also evident from the SEM and TEM micrographs of the sample (Fig. 2a, c). In addition, the adsorption branch is found to increase rapidly at the relative pressure close to unity, which is the characteristic of the isotherms of type II (IUPAC

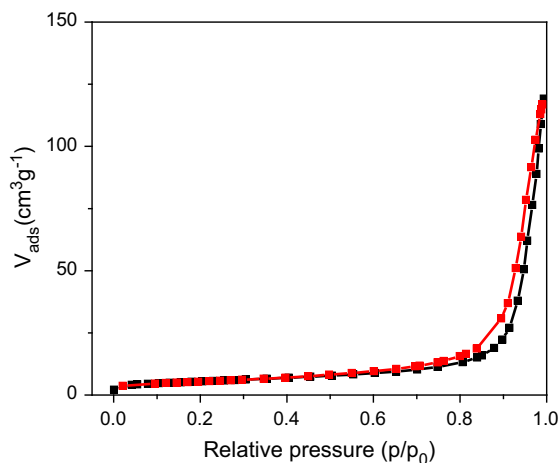


**Fig. 5**  $N_2$  adsorption/desorption isotherm of as-prepared CuS nanocrystals to examine their textural properties

classification) (Sing et al. 1985). The estimated BET specific surface area and pore size for the sample were  $19 \text{ m}^2 \text{ g}^{-1}$  and 16 nm, respectively. While the mixed type II and type IV characteristics of the isotherm indicate the presence of inhomogeneous pore distribution in the sample, type II characteristic at high relative pressure clearly indicates the presence of nonporous, along with macro- and mesoporous, structure of the material. Such an abnormal dual-mode isotherm has been reported for polymeric samples by Van der Vegt et al. (2010) and associated to swelling effect (formation of new pores and dissolution of gas molecules in dense matrix). Jeromenok and Weber have associated this effect to the increased solvation pressure in the matrix, which acts as the driving force for filling the pores with restricted access (Jeromenok and Weber 2013). In the present case, the dual-mode isotherm of the sample can be associated to its typical morphology, formed by the interconnection or aggregation of small nanoparticles.

#### Photocatalytic activity of CuS nanostructures

##### *Photocatalytic degradation vs time*

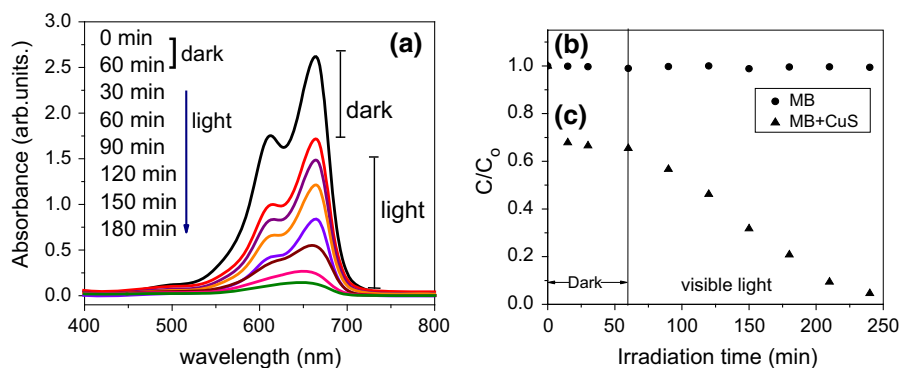
Figure 6a shows the absorption spectra of aqueous MB solution in contact with CuS photocatalyst tested at different intervals. The photocatalytic degradation of MB in the absence and in the presence of CuS nanostructures under visible light irradiation is

displayed in Fig. 6b. As can be seen in Fig. 6a, initially there is a significant decrease in the concentration of MB in the presence of CuS photocatalyst even without illumination. Once the adsorption-desorption equilibrium is reached between catalyst surface and dye molecule under dark condition (30–60 min), the concentration of MB remains almost unaltered (Fig. 6b). In the case of CuS-containing MB solution, there is a sharp decrease in the intensity of 664 nm absorption peak with increasing the illumination time (Fig. 6a). After 90 min of illumination, about 50 % degradation of MB was achieved and nearly a complete (93 %) photodegradation of the dye was attained upon 3-h illumination (see Fig. 6b). However, in absence of photocatalyst, the dye did not undergo any photodecomposition maintaining its concentration practically unaltered even after being exposed to visible light for long time (Fig. 6c).

It is well known that the efficiency of catalytic process is closely related to the specific surface area of the catalyst. The higher the surface area, the larger will be the active sites available for dye molecules, enhancing the adsorption capacity. Xu et al. have reported the photocatalytic degradation of methylene blue over nano-sized  $\text{TiO}_2$  surface demonstrating an increase in the adsorption of MB on the catalyst surface with the increasing surface area (Xu et al. 1999). In our case, the BET surface area of the nanoparticles is not high enough to consider it as the principal factor responsible for high dye adsorption capacity. However, there exists a possibility of the influx of dye solution through the macro- and mesoporous channels formed by the interconnected network. Among the other feasible possibilities, we assume that the high adsorption capacity of CuS in the present experiment is due to the strong interaction between dye molecules and catalyst surface arising from the electrostatic force between the negatively charged CuS surface and cationic dye molecules, such as MB. To confirm our assumption about the negative surface charge of CuS nanoparticles, we have carried out FT-IR spectroscopy and Lewis basicity test on the CuS powder sample, and the results are shown in the following section.

To verify if the Cu ion is leaching during the photocatalytic reaction, the concentration of metal ions was monitored by ICP analysis. The concentration of copper in the reaction solution was below the detection limit of the ICP-AES which firmly suggests

**Fig. 6** **a** MB absorption spectra as a function of illumination time in the presence of CuS photocatalyst. Photocatalytic degradation of MB **b** in absence and **c** in contact with CuS catalyst



that Cu leaching is not occurring or negligible during the photocatalytic reaction. This result is highly relevant from the viewpoint of toxicity concern for using the CuS nanoparticles as a photocatalyst.

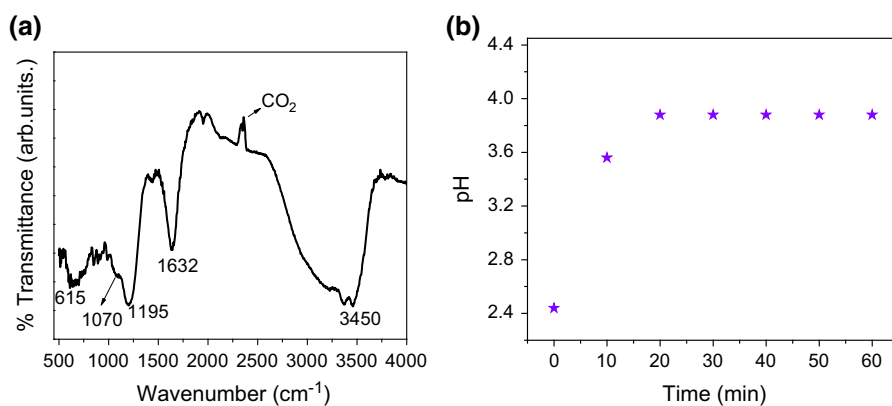
#### FT-IR study and Lewis basicity test to detect hydroxyl ions on CuS surface

Figure 7a displays the FT-IR spectrum of CuS powder. The presence of three bands in the 3200–3500  $\text{cm}^{-1}$  range, which corresponds to the region of stretching vibrations of  $-\text{OH}$  group, can be due to the absorbed water as well as surface-bound hydroxyl ions. The band at 1632  $\text{cm}^{-1}$  corresponds to the  $\text{H}-\text{O}-\text{H}$  bending mode. Water molecule has three normal modes of vibrations, two stretching modes and one bending mode, and hence the third band observed in the stretching region indicates the presence of surface-bound  $\text{OH}^-$  ions, which in turn makes the CuS surface negatively charged (Basu et al. 2010). This point is further discussed below in the section of Lewis basicity test. The band at around 1195  $\text{cm}^{-1}$  is

attributed to C–C skeletal vibration, while the weak shoulder at 1070  $\text{cm}^{-1}$  belongs to C–OH stretching mode of TEA molecule (Gu and Wu 2007; Cao et al. 2006). The appearance of two bands at 1195 and 1070  $\text{cm}^{-1}$  suggests that the CuS surface has been truly modified by TEA with the additional advantage of having extra polar groups, such as  $-\text{OH}$ , coming from triethanolamine (Gu and Wu 2007). Finally, the band at 615  $\text{cm}^{-1}$  is attributed to the Cu–S stretching vibration (Pei et al. 2011). Therefore, the cationic MB molecules preferentially cover the CuS surface which facilitates the electron transfer mechanism in dye degradation process. Basu et al. have also reported a similar phenomenon in the case of MB photodegradation using hexagonal CuS nanoplates as a catalyst and correlated the enhanced catalytic efficiency with the electrostatic interaction between negatively charged catalyst surface and cationic dye molecules (Basu et al. 2010).

The presence of negatively charged hydroxyl ions on CuS surface was further examined qualitatively by performing Lewis basicity test as described in the

**Fig. 7** **a** FT-IR spectrum of CuS sample suggesting the presence of  $\text{OH}^-$  ions on CuS surface, **b** temporal pH variation of the HCl solution after adding CuS powder



experimental section. The rise in pH value of the acid solution during first few minutes on dispersing the CuS powder indicates that there exists a strong electrostatic interaction between  $H^+$  ions of HCl and surface  $OH^-$  ions of CuS (see Fig. 7b). This causes a depletion of protons in the solution resulting in the increase of pH from 2.44 to 3.88. Therefore, it can be concluded that the adsorption of MB on the catalyst surface is due to the electrostatic interaction between the surface  $OH^-$  ions of CuS and cationic MB molecules. The estimated density of  $-OH$  group attached to CuS was  $8.81 \times 10^{11}$  per gram of catalyst (Corro et al. 2014). It is important to mention that CuS is chemically stable in dilute HCl as copper is unable to replace hydrogen due to its position in electrochemical series below hydrogen.

### Photodegradation kinetics

To evaluate the efficiency of CuS as a photocatalyst, we have verified the degradation rate of MB in the catalytic reaction. According to the Beer–Lambert's law, the concentration of MB is linearly proportional to the intensity of absorption peak. Therefore, the decomposition rate of MB can be calculated using the following expression:

$$\text{Degradation (\%)} = \frac{C_0 - C}{C_0} \times 100,$$

where  $C_0$  and  $C$  are the concentrations of dye at  $t = 0$  and at time  $t$ , respectively. Figure 8 shows the degradation rate of MB in the presence of CuS photocatalyst. The decomposition rate increases swiftly at the initial stage of irradiation and then slows down gradually with time achieving practically a complete degradation in 3 h.

In order to understand well the photocatalysis mechanism, the reaction kinetics was investigated using the pseudo-first-order model which is generally applied in the case of low pollutant concentration. The pseudo-first-order equation is given below:

$$\ln C_0/C = kt,$$

where  $k$  is the rate constant of the pseudo-first-order model.

The plot of  $\ln(C_0/C)$  versus irradiation time is shown in Fig. 9. The linear relation between  $\ln(C_0/C)$  and irradiation time indicates that the photocatalytic reaction follows first-order kinetics where the slope

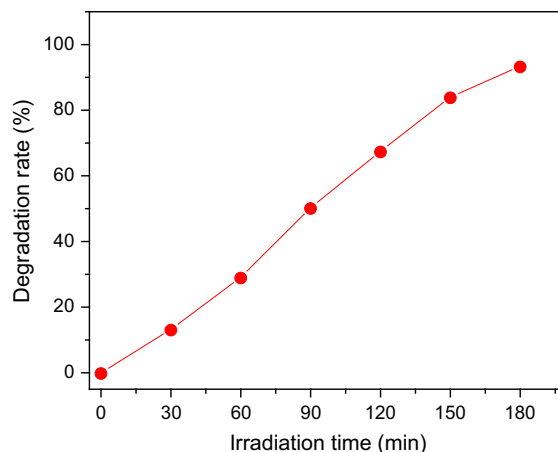


**Fig. 8** Degradation rate of MB over CuS nanostructures at different time intervals

corresponds to rate constant ( $k$ ). As shown in Fig. 9, the experimental data have been fitted well into pseudo-first-order model and give a correlation coefficient ( $R^2$ ) of 0.99699 which is close to 1. The proximity of  $R^2$  value to 1 indicates a good agreement of the model suggesting that the kinetic pathway of dye degradation follows strictly the pseudo-first-order model. The values of  $k$  and  $t_{1/2}$  (half-life) for this catalytic reaction are found to be  $1.58 \times 10^{-2} \text{ min}^{-1}$  and 90 min, respectively. The relatively high value of  $k$  and short half-life time qualify the CuS nanostructures developed in this work as an effective photocatalyst under visible light irradiation.

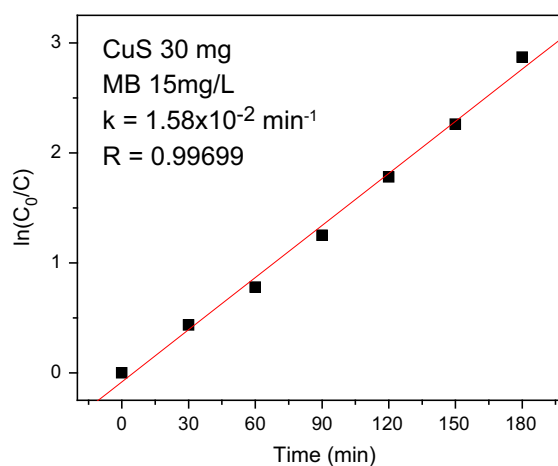


**Fig. 9** Kinetic study for photodegradation of MB with CuS catalyst for pseudo-first-order model

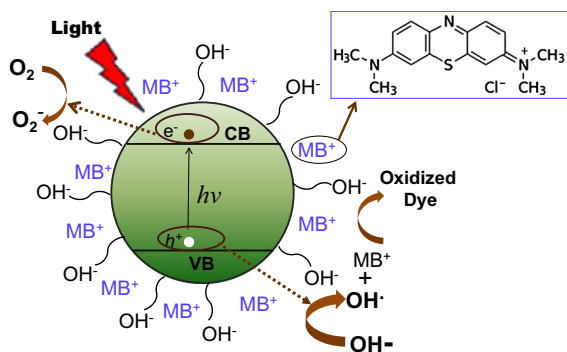
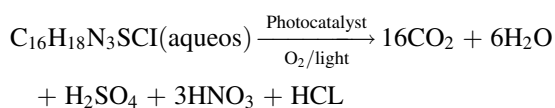


**Fig. 10** Schematic presentation of dye adsorption, photogeneration of electron–hole pairs, and MB photodegradation process on CuS surface

### Mechanism of photodegradation

The mechanism involved in dye decomposition by heterogeneous catalysts has been widely investigated (Linsebigler et al. 1995; Gupta et al. 2012). Initially, the dye molecules are adsorbed on the surface of the photocatalyst. Upon irradiation of CuS nanocrystals, an electron from the valence band gets promoted to the conduction band creating electron–hole pairs. The excited electrons migrate to the catalyst surface and reduce the dissolved oxygen into  $O_2^-$ , while holes participate in the oxidation of the surface-adsorbed water molecules leading to the formation of hydroxyl radicals ( $HO\cdot$ ). As a strong oxidizing species, the so-formed hydroxyl radicals react with dye molecules and potentially oxidize them according to the following chemical reaction (Houas et al. 2001):



A schematic representation of MB adsorption over CuS surface and subsequent dye mineralization upon visible light irradiation has been elucidated in Fig. 10.

### Conclusion

In this paper, we have reported a facile and high-yield synthesis process for producing phase-pure covellite CuS nanoparticles with an average size of 5.0 nm. The structural and optical properties of the powder sample have been thoroughly studied. The band gap energy of

the small CuS nanoparticles shows a weak quantum confinement effect. The visible light-mediated photocatalytic performance of CuS NPs has been verified taking MB as a target contaminant dye. About 93 % MB degradation was achieved with the developed CuS NPs under visible light irradiation during a period of 3 h. The efficient dye degradation capacity of the CuS nanoparticles has been associated with their adequate band gap energy and efficient production of electron–hole pairs under visible light irradiation. The presence of hydroxyl ions at high concentration on the surface of the CuS nanostructures helps adsorb MB molecules facilitating their degradation process under visible light illumination. The evidence of no copper leaching demonstrated by ICP-AES result discards the material safety concerns involved in the use of CuS nanoparticles as a catalyst. The results prove the promising prospect of the synthesized CuS nanostructures as visible-light-sensitive photocatalyst with high adsorptive capacity for large-scale application in wastewater treatment.

**Acknowledgments** Authors thank Dr. J.M. Gracia y Jimenez for providing the FT-IR equipment, and the central laboratory of IFUAP-BUAP for the Raman spectroscopy facility. The technical assistance of Rogelio Moran Elvira in SEM measurement and Ma. Luisa Raman Garcia in XRD analysis has been acknowledged. The CuS nanoparticles used in this work was developed for the projects: Centro Mexicano de Innovación en Energía Solar (CeMIE-Sol 207450/P28), Programa de Apoyo a Proyectos de Investigación e Innovación Tecnológica (PAPIIT-UNAM IN 113214, IN 107815), and Consejo Nacional de Ciencia y Tecnología (CONACyT-238869).

### References

- Basu M, Sinha AK, Pradhan M, Sarkar S, Negishi Y, Govind Pal T (2010) Evolution of hierarchical hexagonal stacked plates of CuS from liquid-liquid interface and its photocatalytic application for oxidative degradation of different dyes under indoor lighting. *Environ Sci Technol* 44: 6313–6318
- Cao JG, Shen M, Zhou LW (2006) Preparation and electrorheological properties of triethanolamine-modified  $TiO_2$ . *J Solid State Chem* 179:1565–1568
- Chen YB, Chen L, Wu LM (2008) Water-induced thermolytic formation of homogeneous core–shell CuS microspheres and their shape retention on desulfurization. *Cryst Growth Des* 8:2736–2740
- Corro G, Bañuelos F, Vidal E, Cebada S (2014) Measurements of surface acidity of solid catalysts for free fatty acids esterification in jatropha curcas crude oil for biodiesel production. *Fuel* 115:625–628

- Daghrir R, Drogui P, Robert D (2013) Modified TiO<sub>2</sub> for environmental photocatalytic applications: a review. *Ind Eng Chem Res* 52:3581–3599
- Deng C, Ge X, Hu H, Yao L, Han C, Zhao D (2014) Template-free and green sonochemical synthesis of hierarchically structured CuS hollow microspheres displaying excellent fenton-like catalytic activities. *Cryst Eng Comm* 16:2738–2745
- Gorai S, Ganguli D, Chaudhuri S (2005) Synthesis of copper sulfides of varying morphologies and stoichiometries controlled by chelating and nonchelating solvents in a solvothermal process. *Cryst Growth Des* 5:875–877
- Gu W, Wu P (2007) FT-IR and 2D-IR spectroscopic studies on the effect of ions on the phase separation behavior of PVME aqueous solution. *Anal Sci* 23:823–827
- Guo Y, Wang L, Yang L, Zhang J, Jiang L, Ma X (2011) Optical and photocatalytic properties of arginine-stabilized cadmium sulfide. *Mater Lett* 65:486–489
- Gupta VK, Pathania D, Agarwal S, Singh P (2012) Adsorptional photocatalytic degradation of methylene blue onto pectin–CuS nanocomposite under solar light. *J Hazard Mater* 243:179–186
- Han Y, Wang Y, Gao W, Wang Y, Jiao L, Yuan H, Liu S (2011) Synthesis of novel CuS with hierarchical structures and its application in lithium-ion batteries. *Powder Technol* 212:64–68
- Hoffmann MR, Martin ST, Choi W, Bahneman DW (1995) Environmental applications of semiconductor photocatalysis. *Chem Rev* 95:69–96
- Houas A, Lachheb H, Ksibi M, Elaloui E, Guillard C, Herrmann JM (2001) Photocatalytic degradation pathway of methylene blue in water. *Appl Catal B* 31:145–157
- Jeromenok J, Weber J (2013) Restricted Access: on the nature of adsorption/desorption hysteresis in amorphous, microporous polymeric materials. *Langmuir* 29:12982–12989
- Jiang X, Xie Y, Lu J, He W, Zhu L, Qian Y (2000) Preparation and phase transformation of nanocrystalline copper sulfides (Cu<sub>9</sub>S<sub>8</sub>, Cu<sub>7</sub>S<sub>4</sub> and CuS) at low temperature. *J Mater Chem* 10:2193–2196
- Kumar P, Gusain M, Nagarajan R (2011) Synthesis of Cu<sub>1.8</sub>S and CuS from copper-thiourea containing precursors; anionic (Cl<sup>-</sup>, NO<sub>3</sub><sup>-</sup>, SO<sub>4</sub><sup>2-</sup>) influence on the product stoichiometry. *Inorg Chem* 50:3065–3070
- Kumar P, Nagarajan R, Sarangi R (2013) Quantitative X-ray absorption and emission spectroscopies: electronic structure elucidation of Cu<sub>2</sub>S and CuS. *J Mater Chem C* 1:2448–2454
- Li HL, Zhu YC, Avivi S, Palchik O, Xiong JP, Kolytyn Y, Palchik V, Gedanken A (2002) Sonochemical process for the preparation of α-CuSe nanocrystals and flakes. *J Mater Chem* 12:3723–3727
- Linsebigler AL, Lu G, Yates JT (1995) Photocatalysis on TiO<sub>2</sub> surfaces: principles, mechanisms, and selected results. *Chem Rev* 95:735–758
- Liu SC, Chen LD, Yao Q, Huang FQ (2008) In situ assembly of Cu<sub>x</sub>S quantum-dots into thin film: a highly conductive p-type transparent film. *J Phys Chem C* 112:12085–12088
- Mane RS, Lokhande CD (2000) Chemical deposition method for metal chalcogenide thin films. *Mater Chem Phys* 65:1–31
- Meng X, Tian G, Chen Y, Zhai R, Zhou J, Shi Y, Cao X, Zhoua W, Fu H (2013) Hierarchical CuS hollow nanospheres and their structure-enhanced visible light photocatalytic properties. *Cryst Eng Commun* 15:5144–5149
- Munce CG, Parker GK, Holt SA, Hope GA (2007) A Raman spectroelectrochemical investigation of chemical bath deposited Cu<sub>x</sub>S thin films and their modification. *Colloids Surf A* 295:152–158
- Nagaveni K, Sivalingam G, Hegde MS, Madras G (2004) Solar photocatalytic degradation of dyes: high activity of combustion synthesized nano TiO<sub>2</sub>. *Appl Catal B* 48:83–93
- Ou S, Xie Q, Ma D, Liang J, Hu X, Yu W, Qian Y (2005) A precursor decomposition route to polycrystalline CuS nanorods. *Mater Chem Phys* 94:460–466
- Panigrahi PK, Pathak A (2013) The growth of bismuth sulfide nanorods from spherical-shaped amorphous precursor particles under hydrothermal condition. *J Nanopart*, Article ID 367812:1–11
- Pei LZ, Wang JF, Tao XX, Wang SB, Dong YP, Fan CG, Zhang QF (2011) Synthesis of CuS and Cu<sub>1.1</sub>Fe<sub>1.1</sub>S<sub>2</sub> crystals and their electrochemical properties. *Mater Charact* 62:354–359
- Qiu X, Miyauchi M, Yu H, Irie H, Hashimoto K (2010) Visible-light-driven Cu(II) – (Sr<sub>1-y</sub>Na<sub>y</sub>)(Ti<sub>1-x</sub>Mo<sub>x</sub>)O<sub>3</sub> photocatalysts based on conduction band control and surface ion modification. *J Am Chem Soc* 132:15259–15267
- Roy P, Srivastava SK (2007) Low-temperature synthesis of CuS nanorods by simple wet chemical method. *Mater Lett* 61:1693–1697
- Safrani T, Jopp J, Golan Y (2013) A comparative study of the structure and optical properties of copper sulfide thin films chemically deposited on various substrates. *RSC Adv* 3:23066–23074
- Setkus A, Galdikas A, Mironas A, Simkieni I, Ankutiene I, Janickis V, Kaciulis S, Mattogno G, Ingo GM (2001) Properties of Cu<sub>x</sub>S thin film based structures: influence on the sensitivity to ammonia at room temperatures. *Thin Solid Films* 391:275–281
- Shen G, Chen D, Tang K, Liu X, Huang L, Qian Y (2003) General synthesis of metal sulfides nanocrystallines via a simple polyol route. *J Solid State Chem* 173(1):232–235
- Shu QW, Li CM, Gao PF, Gao MX, Huang CZ (2015) Porous hollow CuS nanospheres with prominent peroxidase-like activity prepared in large scale by a one-pot controllable hydrothermal step. *RSC Adv* 5:17458–17465
- Sing KSW, Everett DH, Haul RAW, Moscou L, Pierotty RA, Rouquerol J, Siemieniewska T (1985) Reporting physisorption data for gas/solid systems with special reference to the determination of surface area and porosity. *Pure Appl Chem* 57:603–619
- Van der Vegt NFA, Kusuma VA, Freeman BD (2010) Basis of solubility versus TC correlations in polymeric gas separation membranes. *Macromolecules* 43:1473–1479
- Wang X, Xu C, Zhang Z (2006) Synthesis of CuS nanorods by one-step reaction. *Mater Lett* 60(3):345–348
- Wang X, Fang Z, Lin X (2009) Copper sulfide nanotubes: facile, large-scale synthesis, and application in photodegradation. *J Nanopart Res* 11:731–736
- Wu C, Zhou G, Mao D, Zhang Z, Wu Y, Wang W, Luo L, Wang L, Yu Y, Hu J, Zhu Z, Zhang Y, Jie J (2013) CTAB assisted synthesis of CuS microcrystals: synthesis, mechanism, and electrical properties. *J Mater Sci Technol* 29(11):1047–1052

- Xiong S, Xi B, Qian Y (2010) CdS hierarchical nanostructures with tunable morphologies: preparation and photocatalytic Properties. *J Phys Chem C* 114:14029–14035
- Xu N, Shi Z, Fan Y, Dong J, Shi J, Hu M (1999) Effects of particle size of  $\text{TiO}_2$  on photocatalytic degradation of methylene blue in aqueous suspensions. *Ind Eng Chem Res* 38:373–379
- Xu Y, Salim N, Bumby CW, Tilley RD (2009) Synthesis of SnS quantum dots. *J Am Chem Soc* 131:15990–15991
- Zhang W, Wen X, Yang S (2003) Synthesis and Characterization of uniform arrays of copper sulfide nanorods coated with nanolayers of polypyrrole. *Langmuir* 19:4420–4426
- Zhang YC, Du ZN, Li KW, Zhang M, Dionysiou DD (2011) High-performance visible-light-driven  $\text{SnS}_2/\text{SnO}_2$  nanocomposite photocatalyst prepared via in situ hydrothermal oxidation of  $\text{SnS}_2$  nanoparticles. *ACS Appl Mater Interfaces* 3:1528–1537